Hindawi
International Journal of Energy Research
Volume 2024, Article ID 6313421, 17 pages
https://doi.org/10.1155/2024/6313421

Research Article

Optimal Investment Strategy Analysis of On-Site Hydrogen Production Based on the Hydrogen Demand Prediction Using Machine Learning

Hweeung Kwon,[1] **Jinwoo Park**,[2] **Jae Eun Shin**,[3] **and Bonchan Koo**[4]

[1]*Department of Nano Chemical Engineering, Soonchunhyang University, Asan-si, Chungcheongnam-do 31538, Republic of Korea*
[2]*Department of Chemical and Biochemical Engineering, Dongguk University, Seoul 04620, Republic of Korea*
[3]*Future Geo-Strategy Research Center, Korea Institute of Geoscience and Mineral Resources (KIGAM), Daejeon 34132, Republic of Korea*
[4]*Department of Mechanical Engineering, Dong-A University, Busan 49315, Republic of Korea*

Correspondence should be addressed to Jinwoo Park; jinwoop@dgu.ac.kr and Bonchan Koo; bckoo@dau.ac.kr

Received 20 May 2023; Revised 19 November 2023; Accepted 11 December 2023; Published 27 April 2024

Academic Editor: Semen Klyamkin

In order to achieve the hydrogen economy and respond to initial hydrogen demand appropriately, a hydrogen production and operation methodology is required to secure the economic feasibility of long-term on-site HRS. This study proposes a novel investment strategy for on-site hydrogen production to meet future hydrogen demand. The optimal investment strategy based on the dual-modal mode of combined autothermal reforming (ATR) and steam methane reforming (SMR) is proposed for hydrogen production using natural gas (NG) as a raw material. To predict hydrogen demand from 2020 to 2030, the machine learning (ML) technique was adopted. R^2 and MSE as result using ML were 0.9936 and 6.88×10^{-5}, respectively. In addition, the ATR-SMR hydrogen strategy (ASHS) process was analyzed and compared with the SMR-SMR and ATR-ATR hydrogen strategy (SSHS and AAHS) processes in terms of optimal operation rate, storage tank management, economics, and environmental impacts. The operation rate of proposed hydrogen production processes was determined by the hydrogen demand and storage tank level, and the optimal investment plan to install additional hydrogen process depends on the total amount of hydrogen production. In this study, these results were observed due to the effective combination of the strengths of ATR and SMR. Consequently, the ASHS had the best cost-effectiveness (LCOH at \$5.63/kg H_2) and environmental friendliness (unit CO_{2eq} emissions at 10.21 kg CO_{2eq}/kg H_2 and 1.73 kg CO_{2eq}/kg H_2 with CCS). This study includes sensitivity analysis and a comparison of CO_2 taxes by the country for three proposed hydrogen production processes. It could contribute to the optimal operation of the on-site hydrogen production system in preparation for future hydrogen demand.

1. Introduction

Hydrogen is a clean energy carrier with the potential to replace conventional hydrocarbons derived from fossil fuels over the long term. In addition, hydrogen produced from oil refining and petrochemical processes has been widely applied in various chemical plants, power generation, and mobility [1–3]. However, current hydrogen usage has limitations in terms of storage and transportation of large quantities because of the lack of associated technology. Hence, this study proposes an on-site hydrogen refueling station to overcome these issues and attempts to maximize profits by minimizing the operation costs through optimal dual modal process operation considering future hydrogen demand based on machine learning (ML).

Natural gas (NG) and light hydrocarbon are widely used around the world as a raw material for hydrogen production [4, 5]. Hydrogen production technologies can be divided into three representative routes, namely, steam methane reforming (SMR), partial oxidation (POX), and autothermal

reforming (ATR). SMR is currently one of the cheapest hydrogen production technologies [6]. The advantages of SMR are its relatively high operational efficiency and low production cost. However, SMR requires a high temperature (approximately more than 500°C), which is based on conventional hydrocarbons owing to the endothermic reaction [7, 8]. The required energy is supplied to the system from an external heat source. The thermal efficiency of the general SMR in industrial processes has a range of 70–85% [9]. ATR involves the addition of catalytic POX to the SMR process. ATR involves both an endothermic reaction of SMR and an exothermic reaction of POX, which occurs simultaneously. Therefore, the temperature distribution of ATR sharply increases in the thermal section by an exothermic reaction, and then constantly decreases in the catalytic section by an endothermic reaction. No additional heat was required due to this phenomenon. Kim et al. [10] investigated the start-up period of fermentation hydrogen production. They overcame fluctuations in hydrogen production for 10 days and stabilized hydrogen production. Kiaee et al. [11] demonstrated the operating performance of a pressurized alkaline electrolyzer in a hydrogen refueling station (HRS), under various operation modes. This paper provided an acceptable control strategy for system operation considering electrolyzer characteristics when integrating the electrolyzer loads in the power system. Genovese et al. [12] investigated the standard operation of an HRS with on-site hydrogen production using water electrolysis. The standard operation and maintenance operation were investigated using calculation, mathematical modeling, and analysis based on the database. They found that operation strategy could lower the average loss ratio of hydrogen from 30-35% to 2-10%. Xu et al. [13] developed a renewable energy hub framework with optimal operation using multiple energy supplies, considering production, conversion, and storage costs. The proposed methodology was applied to community microgrids under grid-connected and grid-disconnected modes, and the operation costs based on solar-wind accommodation could be improved by up to 1.59% compared to the previous system. Samsatli et al. [14] developed a novel optimization model for the operation and design of an integrated electricity system for a hydrogen-wind network. This optimization model could be determined by the location and size of the plant, storage, and transportation technologies. Kim and Kim [15] developed strategic planning using the optimization of a hydrogen supply system with a renewable source. This optimization model was applied to the wind-powered hydrogen supply system and analyzed cost drivers. In addition, they developed regulation policies based on various scenarios. Liu et al. [16] carried out optimal planning for a distributed energy system based on hydrogen, which adjusted to various energy supply and demand. They minimized the capital expenditure (CAPEX) and operating expenditure (OPEX) of the system using multi-energy storage units. Compared to the conventional electricity-driven energy system, CO_2 emissions could be reduced by more than 100% in high solar radiation areas, and OPEX is reduced by a maximum of 60%. Wu et al. [17] proposed a novel scheduling model for microgrids with hydrogen-fueling stations under uncertainty such as renewable energy power and electrical hydrogen load. This study applied a robust optimization technique, and the results present that the distributed energy resources and hydrogen-fueling stations were optimally adjusted.

As the current infrastructure for hydrogen is generally insufficient, it is important to secure economic feasibility from hydrogen production to hydrogen charging at the HRS. Jang et al. [18] carried out a technoeconomic analysis of various hydrogen production technologies based on the Monte Carlo method. The levelized cost of hydrogen (LCOH) was determined by two dominant variables such as electricity cost and tax rate. Restrepo et al. [19] performed a technoeconomic evaluation of hydrogen production based on renewable energy and developed a novel methodology for the operation of several reactors. This study shows that the efficiency from the sun to hydrogen production was obtained at 31.8%, and LCOH presents \$4.55/kg H_2.

Global greenhouse gas emissions cause climate change from energy consumption with fossil fuels. Therefore, most countries are trying to reduce GHGs. Most hydrogen production processes (HPPs) currently generate very high CO_2 emissions as raw materials and fuel are used without deploying a carbon capture system. A carbon capture and storage (CCS) system is one of the important methods to reduce CO_2 emissions. The optimal location of the CCS in the HPP could be significantly improved in reducing CO_2 emissions. They provided an optimal steam-to-carbon (S/C) ratio to reduce CO_2 emissions and investigated oxygen enrichment effects in the furnace to improve CO_2 capture performance [20]. Air products carried out a carbon capture and sequestration project to develop a new retrofit system to capture CO_2 generated from industrial SMR plants. CO_2 has been concentrated from 15% to at least 98% of the waste stream from SMR, resulting in a reduction of more than 1 million tons of CO_2 emissions per year [21]. The traditional HPPs use NG as a raw material and fuel. It is generally known to emit approximately 9 to 11 kg CO_2 per 1 kg H_2 [22]. Meanwhile, the hydrogen production via SMR with CCS was investigated at 3.9 kg CO_2 per 1 kg [23]. Oni et al. [24] carried out a comparative assessment of ATR with CCS to produce blue hydrogen. They achieved low GHG emissions and 3.91 kg CO_{2eq}/kg H_2 and demonstrated that the economic feasibility of SMR plants depends on the CO_2 capture rate. Granovskii et al. [25] conducted a study on GHG emissions from hydrogen production and evaluated the economic aspects of using renewable energy instead of fossil fuels. To evaluate the economic, social, and environmental impacts, Acar and Dincer [26, 27] compared and analyzed different hydrogen production methods based on renewable and nonrenewable sources. In addition, they evaluated the environmental, economic, social, and technical performance of hydrogen production, including sources, systems, and storage options. They proposed reliable guidelines for evaluating the hydrogen production options. Hong et al. [28] developed a multiobjective optimization model for on-site SMR hydrogen production to reduce CO_2 emissions. The thermal efficiency reached between 77.5 and 87.0%, and CO_2 emissions indicated between 577.9 and 597.6 tons per year through Pareto-optimal solutions. Furthermore, some researchers have used modeling and optimization of

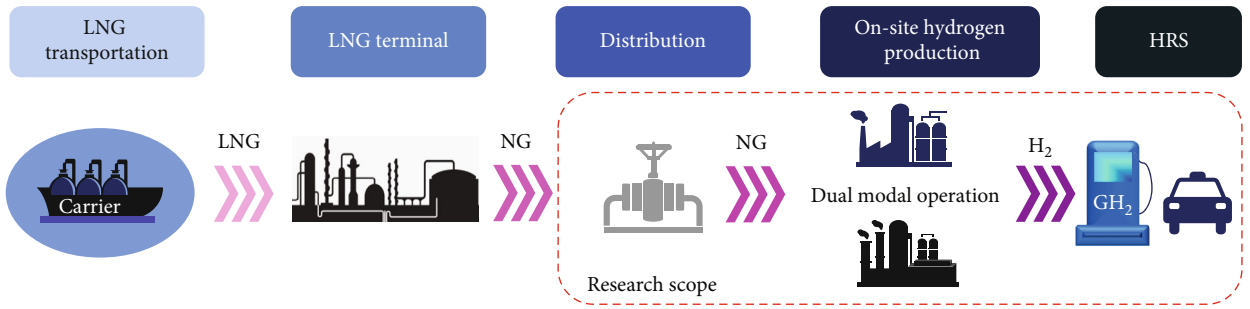

Figure 1: Overview of integrated on-site hydrogen production system and HRS.

processes using ML. Lee et al. [29] performed energy optimization using ML for on-site hydrogen production. They optimized the operating conditions of SMR, and thermal efficiency shows 85.6%. In order to increase the energy efficiency of hydrogen production, Strusnic and Avsec [30] developed integrating new technologies based on the thermochemical Cu-Cl cycle using the exergoeconomic machine-learning method. Haq et al. [31] analyzed the prediction and evaluation of hydrogen yield through combined ML methods and genetic algorithms. The coefficient of determination (R^2) and root mean square error (RMSE) values of predicting hydrogen yield with Gaussian process regression (GPR) were showed 0.997 and 0.093, and these values indicate that the proposed model is appropriate for dealing with complex variable-target correlation. Pourali and Esfahani [32] carried out a performance evaluation for an integrated hydrogen production system based on an analytical approach and ML. In addition, they provide appropriate correlations for mixture properties and the heat of reactions based on the decision tree algorithm. Ozbas et al. [33] analyzed hydrogen production from biomass gasification using ML methodology. In order to achieve the goal, they performed hydrogen concentration prediction using k nearest neighbors (KNN), support vector machine (SVM), and decision tree (DT). Vo et al. [34] investigated an integrated approach based on mathematical modeling and artificial neural network (ANN) for SMR. This study developed a hydrogen production system using operational optimization and design at a low computational cost. Koo et al. [35] inferred the operating parameters of SMR from the temperature field by utilizing ML and proper orthogonal decomposition (POD). The authors used the reduced order model technique based on POD to extract the low-rank features from the training dataset to deal with the high dimensional data resulting from computational fluid dynamics.

Previous studies have focused on optimizing operation conditions in single hydrogen production process (HPP) such as SMR and ATR or developing integrated processes. However, these studies mainly aim to increase system efficiency, life cycle assessment analysis based on renewable energy, and performance evaluation of HPP by using the ML technique. However, few studies on the hydrogen production and operation methodology of on-site HRS for vehicles consider the initial hydrogen demand to achieve the hydrogen economy. Hence, the optimal hydrogen production method in on-site HRS is essential to respond to initial hydrogen demand and secure economic feasibility. The objective of this study was to establish optimal operation strategy and hydrogen storage tank management strategies for the proposed on-site hydrogen production system in response to hydrogen demand. First, the future hydrogen demand in this study was predicted using ML techniques such as ANN. After the prediction, three conceptual designs were developed for on-site HRS based on the operation of dual-modal mode. To secure economic feasibility, the proposed optimal operation and storage tank management strategies were analyzed for the LCOH, CAPEX, and OPEX. The CO_2 emissions from each system were determined to evaluate its environmental impact. Furthermore, this study performed a sensitivity analysis for various descriptors, an LCOH analysis over the operation period, and a carbon tax for various countries. Figure 1 presents a comprehensive overview from liquefied natural gas (LNG) import to charge gas hydrogen (GH_2) at HRS in this study.

2. Problem and Process Description

2.1. Problem Description. Nowadays, to achieve a hydrogen economy, efficient infrastructure is required to charge hydrogen to hydrogen vehicles considering the increasing number of hydrogen vehicles. The HRS is classified as on-site and off-site HRSs, according to the hydrogen supply method. An off-site HRS is a system in which hydrogen is produced from an oil refinery, petrochemical plant, or hydrogen production plant that is transported to the HRS using a tube trailer, stored, and charged to hydrogen vehicles. If the demand for the transportation of hydrogen is low, this supply system is an appropriate method in terms of economics. However, this approach no longer becomes a lucrative model owing to the continuously increasing future hydrogen demand. Hence, the integrated on-site hydrogen production system using natural gas and HRS is required from a long-term perspective. In general, if the transportation distance from the hydrogen production source to the HRS is long, and it is easy to supply natural gas, an on-site hydrogen production system in HRS is preferred. The representative hydrogen production method includes SMR and ATR. SMR is not suitable as an early model with low hydrogen demand because it requires long start-up and shutdown times due to high-temperature operation. In addition, the operation rate should be maintained as much as possible because frequent start-up/shutdown cycles can significantly reduce production efficiency [36]. However, ATR is

relatively easier to operate than SMR and has very short start-up and shutdown times [37]. Therefore, it is possible to adjust the operation rate for hydrogen production through ATR, and if hydrogen production is excessive, the hydrogen demand can be managed by supply control through process shutdown. If the demand for hydrogen increases sharply, SMR and ATR are simultaneously operated. SMR produces hydrogen continuously, and an insufficient amount of hydrogen is produced by changing the ATR operation mode. A schematic of the proposed process depicts Figure S1 in supplementary information (SI).

2.2. Process Description. Conventional hydrogen production methods, such as SMR and ATR, consume NG as the raw material. Generally, the stream from the NG pipeline first passes through the pretreatment unit because NG contains an odorant such as sulfur. The catalysts for SMR and water gas shift (WGS) are very sensitive to sulfur. Hence, the sulfur contained in NG must be removed using a pretreatment unit such as desulfurization equipment. The mainstream then enters the prereformer (PR). The PR plays a very important role in converting the heavy hydrocarbons of NG to methane at a temperature range of 350 to 550°C. The mainstream exiting the PR is heated from the external heating source and passes through the main reactors (SMR and ATR).

2.2.1. SMR Process with WGS Unit. The main chemical reactions to produce hydrogen occur in SMR. These reactions are accompanied by an optimal catalyst for increasing the hydrogen production rate. The catalyst used in the SMR reaction is generally in the powder form of the Ni-base. Ni-catalyst is widely used in industrial SMR processes and could prevent sintering and carbon deposition under high temperatures [38]. In addition, this reaction requires high heat from an external source owing to the endothermic phenomenon of steam reforming. NG and high-temperature steam react at approximately 850-900°C in the SMR reactor, producing a mixture of CO, H_2O, CH_4, and H_2 [39].

$$\begin{aligned} CH_4 + H_2O &\leftrightarrow 3H_2 + CO \quad \Delta H^o_{298K} = +206\,\text{kJ/mol} \\ CH_4 + 2H_2O &\leftrightarrow 4H_2 + CO_2 \quad \Delta H^o_{298K} = +164.9\,\text{kJ/mol} \end{aligned} \tag{1}$$

To produce additional hydrogen, the stream exiting the SMR reactor passes through the WGS reactor. Here, additional hydrogen is produced by the WGS reaction of CO and H_2O at 300°C. This CO shift reaction is slightly exothermic as shown in the following equation [40]:

$$CO + H_2O \longrightarrow CO_2 + H_2 \quad \Delta H^o_{298K} = -41.1\,\text{kJ/mol} \tag{2}$$

2.2.2. ATR Process with WGS Unit. ATR consists of combustion and catalytic zones, and the combustion zone partially oxidizes NG, whereas steam enters the catalytic zone at high temperatures. Therefore, the reactions in the combustion and catalytic zones were simultaneously activated. The high-temperature heat generated by the combustion reaction was used for the catalytic reaction. In particular, flue gas is no longer generated because oxidation takes place within the reactor. The operating conditions of ATR have a relatively high temperature (900–1150°C) compared to SMR. In addition, if the steam-to-carbon ratio is reduced, the conversion efficiency can be increased. The use of air as the feed for oxygen is economical and convenient. However, a large amount of N_2 was produced as a by-product. Therefore, an air separation unit (ASU) was necessary to supply pure O_2 to the process to increase the reaction efficiency. The mixed stream of NG and high-temperature steam are heated to approximately 950°C using the heater and then entered into the ATR reactor, and three major reactions are presented in the following equations [41]:

$$\begin{aligned} CH_4 + \frac{3}{2}O_2 &\leftrightarrow 3H_2O + CO \quad \Delta H^o_{298K} = -520\,\text{kJ/mol} \\ CH_4 + 2H_2O &\leftrightarrow 4H_2 + CO_2 \quad \Delta H^o_{298K} = +164.9\,\text{kJ/mol} \\ CO + H_2O &\longrightarrow CO_2 + H_2 \quad \Delta H^o_{298K} = -41.1\,\text{kJ/mol} \end{aligned} \tag{3}$$

The mainstream exiting the ATR reactor passes through the WGS reactor and produces additional hydrogen. Finally, to obtain the highest hydrogen purity, syngas travels through the pressure swing adsorption (PSA) unit. PSA is generally aimed to recover approximately 90% of hydrogen. PSA is operated using periodic pressure changes, and impurities are removed by adsorption and desorption. The capacity of the PSA unit is determined based on the amount of impurities such as CO_2, CO, and N_2 removed from the syngas. The tail gas from PSA and exhaust gas from the furnace were mixed and transferred to CCS to capture CO_2. The top outlet stream of the absorber, including high-caloric components such as CH_4 and H_2 in the CCS system, was sent to the furnace. The hydrogen purity grade exiting from PSA is expressed as a standard decimal notation, and the hydrogen purity of vehicles is generally 99.9995%.

This study proposes a novel conceptual design to achieve optimal operational performance considering future required hydrogen demand. The hydrogen of the proposed HPPs is produced using an on-site hydrogen production method according to hydrogen demand. The total production capacity of the proposed system is 600 Nm^3/h. SMR and ATR in this model produce hydrogen in parallel at the same time. When the hydrogen demand is low, hydrogen is first produced using ATR, which is easy to operate; when a large amount of hydrogen is required, SMR begins to operate.

3. Methodology

3.1. Hydrogen Demand Prediction Based on the ML Technique. In this study, the future demand for hydrogen was predicted using an artificial neural network (ANN) algorithm for ML, as shown in Figure 2. The major factors included the number of vehicles registered by region, the amount of by-product hydrogen from refineries and petrochemical plants, vehicle mileage by region, and fuel efficiency by vehicle type. All descriptors were listed at monthly intervals from January 2015 to December 2018. In addition, the dataset of this study had 48 points. Major data, such as vehicle registration and mileage by region, were

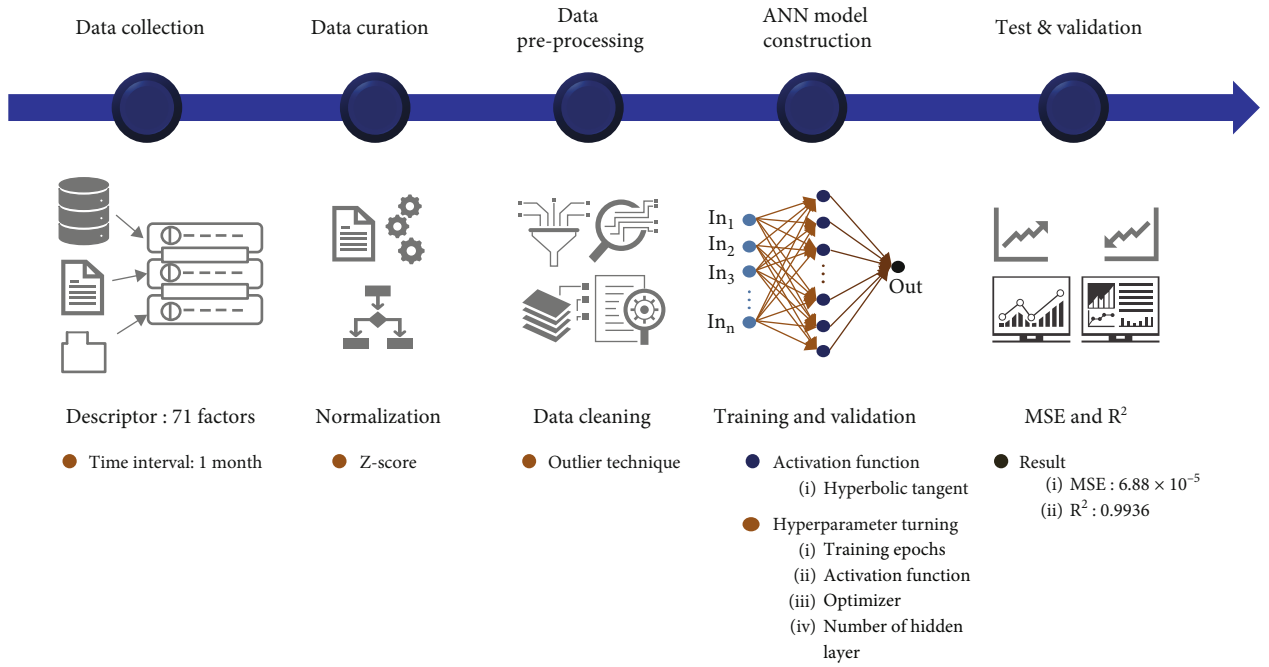

Figure 2: Structure of the proposed ANN for the hydrogen demand prediction.

obtained from the official Korean government database. A prediction model was developed based on the collected data. The accuracy of the prediction model mainly depends on the quantity and quality of the data. To obtain high-quality data, the data were normalized such that the information could be clearly displayed and defined [42–44]. This study also applies an outlier removal technique to remove irrelevant data. To determine an outlier, a threshold point is required that has a distinguishing feature compared to normal data. Hence, this study applied Z-score normalization as a statistical methodology with a probability distribution. The Z-score normalization is shown in the following:

$$Z_i = \frac{x_i - \bar{x}}{S} (i = 1, 2, 3, \cdots, n), \tag{4}$$

where $\bar{x}$ is the mean of the data, S is the standard deviation of the data, and x_i is the data points of the descriptors. As the value of $|Z_i|$ increased, the outlier probability of the data point increased. ANN model is learned through loss function. The loss function is a method to evaluate a particular algorithm model fit with a given data. This study adopted mean squared error (MSE) as a loss function and R^2 as an indicator of the performance to secure the reliability of ANN. However, an overfitted model can show a high R^2 value. MSE and R^2 are as follows:

$$\begin{aligned} \mathrm{MSE} &= \frac{1}{n} \sum_{i=1}^{n} (y_i - \hat{y}_i)^2, \\ R^2 &= \frac{\sum_{i=1}^{n} (y_i - \hat{y}_i)^2}{\sum_{i=1}^{n} (y_i - \bar{y}_i)^2}, \end{aligned} \tag{5}$$

where n is the total number of considered data to learn ANN model. y_i and $\hat{y}_i$ indicate actual and predicted values of the i th data. $\bar{y}_i$ is the average value of total data.

In order to minimize the loss function or to maximize the efficiency of production, the ANN model was composed of feedforward using a multilayer perceptron based on a backpropagation algorithm using a gradient descent optimizer and was trained using supervised learning. ANN model was developed to predict hydrogen demand. The input variables were considered as the daily mileage of vehicles such as cars, buses, and trucks, the fuel efficiency of fuel cell electric vehicles, the amount of by-product hydrogen supply from petrochemicals and refineries, and the number of vehicles registered for each region. In this study, the input descriptors were 71 (see Table S1 in SI), and the output of this model is one. The outputs obtained for future hydrogen demand will be subjected to the ANN modeling with 70% for training and 30% for validation. In addition, the number of hidden layers was set to 4. Furthermore, the hyperparameters, including training epochs, activation function, number of neurons for the hidden layer, and the optimizer were tuned and applied. Specifically, Levenberg-Marquardt (LM) and sigmoid are used for the training algorithm and activation function, respectively.

3.2. Optimization Model for Hydrogen Investment Strategy. The operating rate of HRS for hydrogen production relies on hydrogen demand. However, future hydrogen demand includes uncertainty and volatility. Hence, the optimal production strategy for HPP is required. In general, an on-site hydrogen production system with HRS produces hydrogen considering hydrogen demand and storage tank capacity. The hydrogen tank is used for storage, to charge vehicles from the high-pressure tank, and plays an important role

as a buffer. Generally, the hydrogen storage tanks in HRS were pressurized to 25 MPa, 35 MPa, or 70 MPa [45]. The proposed integrated on-site hydrogen production system and HRS provide the optimal operation rate considering the hydrogen demand and input data change every month. The optimization predicts the monthly usage for each month based on hydrogen demand data over the years, which is used to determine the optimal operation rate and storage tank management per month. The optimization is performed for a specified period, and the hydrogen demand can determine an optimal operation pattern for an on-site HRS. Table 1 shows the assumptions used to analyze the economic feasibility.

The objective function is to maximize the total profit, which is calculated by

$$\begin{aligned} &\text{Objctive function}: \max.\text{profit} = \sum_{t\in T} \text{MP}_t, \forall t \in T, \\ &\text{subject to } \text{TS}_t^L \le \text{TS}_t \le \text{TS}_t^U, \\ &\quad \text{OR}_t^{\text{SMR},L} \le \text{OR}_t^{\text{SMR}} \le \text{OR}_t^{\text{SMR},U}, \\ &\quad \text{OR}_t^{\text{ATR},L} \le \text{OR}_t^{\text{ATR}} \le \text{OR}_t^{\text{ATR},U}, \\ &\quad \text{APH}_t < \text{RH}_t + 0.9\text{TS}_t. \end{aligned} \tag{6}$$

$\text{OR}_t^{\text{SMR},L}$ and $\text{OR}_t^{\text{SMR},U}$ are the lower and upper bounds of the operation rate for SMR during the period t. $\text{OR}_t^{\text{ATR},L}$ and $\text{OR}_t^{\text{ATR},U}$ are the lower and upper bounds of the operation rate for ATR during the period t. cc and TS_t^U are lower and upper bounds of the level of the storage tank during the period t. RH_t is amount of required hydrogen production per month. The lower and upper bound values of the storage tank and operation rates of SMR and ATR are provided in Table S5 of SI.

$$\text{MP}_t = \text{TP}_t\text{-TI}_t\text{-OC}_t\text{-RM}_t, \tag{7}$$

where TP_t, TI_t, OC_t, and RM_t represent total profit, annualized total investment costs, operation cost, and raw material cost, respectively.

$$\text{TP}_t = \text{HS}_t \times \text{AH}_t, \tag{8}$$

where HS_t and AH_t indicate hydrogen selling price and amount of hydrogen sales, respectively.

The operation cost consists of maintenance, labor, and other costs.

$$\text{OC}_t = \text{CM}_t + \text{CL}_t + \text{COT}_t, \tag{9}$$

where CM_t and CL_t represent maintenance and labor costs, respectively. COT_t denotes other costs during the period t.

$$\begin{aligned} \text{RM}_t &= \text{CR}_t \times \text{AR}_t, \\ \text{AR}_t &= \sum_{j\in J} \left(\text{AN}_{j,t} + \text{AF}_{j,t}\right), \end{aligned} \tag{10}$$

Table 1: Assumptions for economic evaluation [46–48].

Parameter	Value	Unit	
Natural gas	500	\$/ton	
Electricity	0.06	\$/kwh	
Process water	2.73	\$/ton	
Cooling water	1.34	\$/ton	
Maintenance	3	%	Annualized capital cost
Plant life	20	yr	
Tax rate	25	%	
Discount rate	7	%	
Others	1	%	Annualized capital cost

where CR_t and AR_t represent the raw material price as raw material and the total amount of raw material during time period t, respectively. $\text{AF}_{j,t}$ denotes the amount of used NG to maintain the reaction temperature of reactors by hydrogen production types j during time period t.

The amount of stored hydrogen in the storage tank was calculated as follows:

$$\text{TS}_t = \text{TS}_{t\text{-}1} + \text{APH}_t\text{-AH}_t, \tag{11}$$

where TS_t indicates the amount of stored hydrogen in the storage tank, TS_{t-1} presents the amount of storage in the hydrogen tank from the previous month, and APH_t indicates the amount of hydrogen production during the period t.

The amount of hydrogen produced per month was the sum of the amounts of hydrogen produced by SMR and ATR. In addition, the amount of hydrogen produced from SMR and ATR is expressed as the product of the conversion rate from NG to hydrogen, operation rate, and amount of NG input for each process.

$$\begin{aligned} \text{APH}_t &= \sum_{j\in J}^{J} \text{AP}_{j,t}, \\ \text{AP}_{j,t} &= \sum_{j\in J}^{J} \left(\text{AN}_{j,t} \times \text{CR}_{j,t} \times \text{OR}_{j,t}\right), \end{aligned} \tag{12}$$

where $\text{AP}_{j,t}$ denotes the amount of produced hydrogen by hydrogen production types j during time period t. $\text{AN}_{j,t}$, $\text{CR}_{j,t}$, and $\text{OR}_{j,t}$ indicate the amount of NG inputs, conversion rate, and operation rate by hydrogen production types j during time period t, respectively.

3.3. Economic Analysis. The economic analysis of proposed HPPs is performed to select the optimal HPP based on the CAPEX and OPEX. CAPEX consists of direct costs, including equipment purchase and installation costs, and indirect costs containing contingency and licensing fees as shown in Eq. (13). In addition, in order to estimate the equipment purchase cost for a different size, the six-tenths rule was adopted in this study, as formulated in Eq. (14). This cost estimation method provides very reliable results when only

an approximate cost is required within ±20%. OPEX consists of variable costs (e.g., raw materials, utility, and labor costs) and fixed costs (e.g., maintenance, insurance, and depreciation costs) [46].

$$\mathrm{CAPEX}_{\mathrm{total}} = \mathrm{CAPEX}_{\mathrm{direct}} + \mathrm{CAPEX}_{\mathrm{indirect}}, \tag{13}$$

$$C_b = C_a \left(\frac{S_b}{S_a}\right)^{\alpha} \left(\frac{\mathrm{CEPCI}_{\mathrm{tar}}}{\mathrm{CEPCI}_{\mathrm{ref}}}\right), \tag{14}$$

$$\mathrm{OPEX}_{\mathrm{total}} = \mathrm{OPEX}_{\mathrm{variable}} + \mathrm{OPEX}_{\mathrm{fixed}}, \tag{15}$$

where C_b and C_a are approximate and reference costs of main equipment, respectively. S_b and S_a are the target and reference sizes of the main equipment, respectively. α indicates a scaling factor, and its value is 0.6. $\mathrm{CEPCI}_{\mathrm{tar}}$ and $\mathrm{CEPCI}_{\mathrm{ref}}$ present the chemical engineering plant cost index of the target year and reference year, respectively.

Furthermore, the LCOH is calculated by dividing the total annual expenditure by the amount of annually produced hydrogen, as shown in the following:

$$\begin{aligned} \mathrm{LCOH} &= \frac{\mathrm{CAPEX}_{\mathrm{ann}} \times \mathrm{CRF} + \mathrm{OPEX}_{\mathrm{ann}}}{P_{\mathrm{H_2}}}, \\ \mathrm{CRF} &= \frac{i \times (1+i)^{\mathrm{PL}}}{(1+i)^{\mathrm{PL}} - 1}, \end{aligned} \tag{16}$$

where CRF, i, PL, and $P_{\mathrm{H_2}}$ denote the capital recovery factor, the interest rate, plant life, and the total amount of produced H_2, respectively.

3.4. Environmental Analysis. The environmental evaluation of this study was conducted based on unit CO_2 equivalent emissions per kg H_2. Most of the CO_2 emissions are generated by SMR and WGS reactions and by burning fuel gas in the furnace to maintain a reforming reaction environment. However, this environmental evaluation does not consider the CO_2 emissions captured in the CCS. The unit CO_{2eq} emissions could be expressed as in

$$\mathrm{Unit\ CO_{2eq}\ emissions} = \frac{\mathrm{total\ direct\ CO_2\ emissions}}{\mathrm{amount\ of\ produced\ hydrogen}}. \tag{17}$$

4. Results and Discussions

This study considers the operation methodology for three proposed HPPs (ATR-SMR, SMR-SMR, and ATR-ATR) to maximize the total profit during a given period through hydrogen demand, prediction using an ML technique. The investment plan of the established model was determined considering the operation rate of the on-site hydrogen production and the amount of hydrogen production. In addition, an economic evaluation was carried out in terms of LCOH based on CAPEX and OPEX. Furthermore, CO_2 emissions during the production of hydrogen were calculated based on the optimal operation in the three proposed HPPs.

4.1. Simulation Result. The simulation in this study was performed assuming that the on-site hydrogen production system was operated at 100% capacity. Figure 3 shows the process flow diagram (PFD) of ASHS for the simulation, along with the major streams and major stream information summarized in Table S2 in SI. In addition, PFD and major stream information of SSHS and AAHS are summarized in Figures S2-S3 and Tables S3-S4, respectively. This study considered an annual hydrogen production of approximately 1.29 tons per day (TPD) in an on-site hydrogen production system. The required NG and H_2O feeds for the hydrogen production process were 10.56 and 21.23 kmol/h, respectively. In the SMR process, the NG and H_2O mixed feed goes through the PR after its temperature is increased to 501°C using an external heating source. The PR plays a major role in the conversion of heavy hydrocarbons to methane. The outlet stream from the PR entered the separator to separate the unreacted heavy hydrocarbons and nitrogen. The flow rate of the outlet stream from the separator was 14.16 kmol/h, and the mole fraction of CH_4 was increased to 0.2651. Then, to meet the SMR operating conditions, the temperature of stream "7" was increased to 750°C using an external heating source. In the SMR reactor, the reaction is performed to produce hydrogen at high temperature and pressure using a Ni-based catalyst. The flow rate of the outlet stream from SMR was 21.67 kmol/h, and the mole fraction of hydrogen was 0.6749. Most of the CH_4 was converted to H_2 and CO, and a small amount of methane remained unreacted owing to the insufficient conversion rate. To produce additional hydrogen, the temperature of stream "8" was decreased by 300°C to satisfy the WGS operating condition, it entered the high-temperature shift (HTS) reactor of the WGS, and then passed through the low-temperature shift (LTS) reactor again. In the WGS reactor, the mole fraction of H_2 increased from 0.5194 to 0.6749. Water was removed from the stream using a separator before entering the PSA. Then, 13.33 kmol/h of pure hydrogen was produced through PSA, and 5.264 kmol/h of tail gas was sent to the furnace. The CO_2 from tail gas was separated by PSA and then mixed with exhausting gas which is discharged from the furnace. The mixed steam is sent to CCS to capture CO_2, and approximately 83% of CO_2 is captured in CCS. After being captured from CCS, the remaining gas enters the furnace and is used as a heat source for the system. On-site hydrogen production using ATR also produces hydrogen in a procedure similar to SMR. The remarkable difference compared to SMR is that the temperature should be raised to approximately 1050°C to satisfy the operating conditions of ATR for hydrogen production, as shown in the information of stream "11."

4.2. Hydrogen Demand Prediction. To achieve high accuracy in hydrogen demand prediction, outlier removal was performed using Z-score normalization for data preprocessing. The preprocessing method using the outlier technique is as follows. First, the upper and lower limits of the data were set. Then, (1) if the data points were lower than the lower

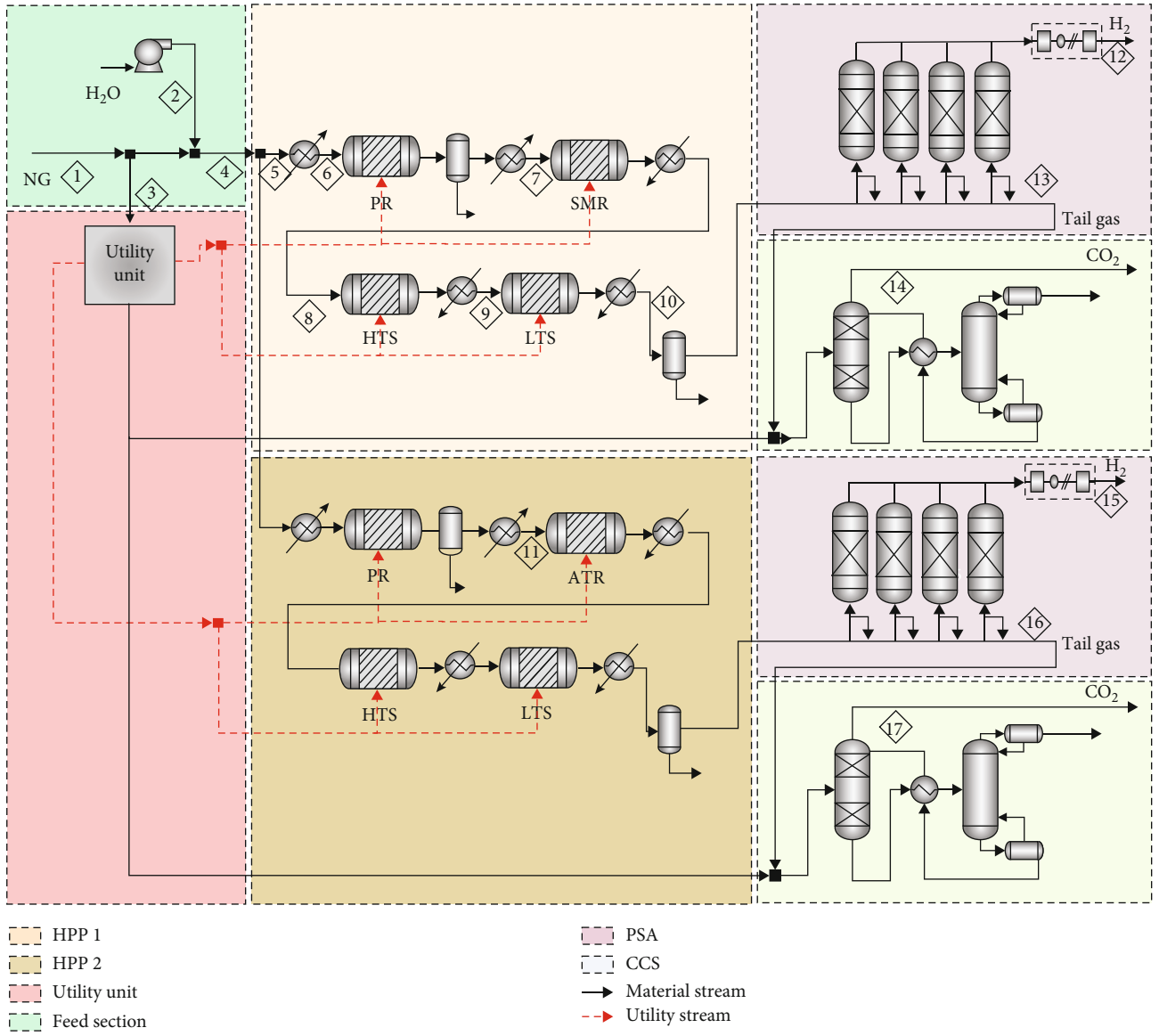

Figure 3: Conceptual design and stream information of dual-modal operation for hydrogen production.

limit, they were replaced with the lower limit value, and (2) if the data points were higher than the higher limit, they were replaced with the higher limit value. In addition, to minimize errors in ANN prediction, hyperparameter tuning plays an important role in determining the number of optimal epochs and determining early stopping. Furthermore, the number of hidden layers was determined for the high performance of the ANN. Finally, the predicted output value was calculated using the four hidden layers used for the hyperbolic tangent transfer function. Figure 4 shows the results of applying the preprocessing and hyperparameter tuning techniques with random search. The error between the predicted and actual values can be confirmed through data preprocessing and hyperparameter tuning techniques. This ANN model is retrained until the coefficient of determination for validation is more than 0.99 and the mean square error (MSE) is less than 10^{-4}. As a result, the R^2 and MSE values were 0.9936 and 6.88×10^{-5}, respectively. This means that the actual and predicted values match very well without overfitting the data. Using the aforementioned techniques, the performance of the ANN model was significantly improved, whereas the original data-based model showed an R^2 of 0.8951.

The number of on-site HPP with HRS is calculated by dividing predicted hydrogen demand by the amount of one on-site hydrogen production. The number of hydrogen production system with HRS required based on the predicted hydrogen demand is depicted in Figure S4 in SI.

$$\mathrm{HRS}_{\mathrm{num}} = \frac{H_d}{O_{\mathrm{hp}}}. \tag{18}$$

It shows an exponential tendency in which the hydrogen demand drastically increases by approximately 10 times over the next 10 years. The generated data imply that the

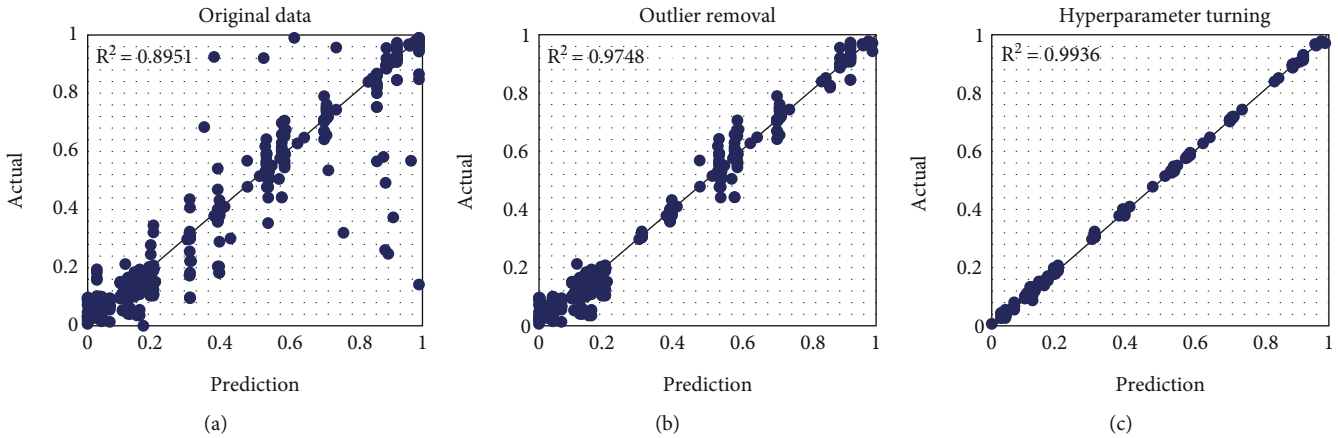

Figure 4: Data arrangement with (a) original raw data, (b) outlier removal, and (c) hyperparameter tuning.

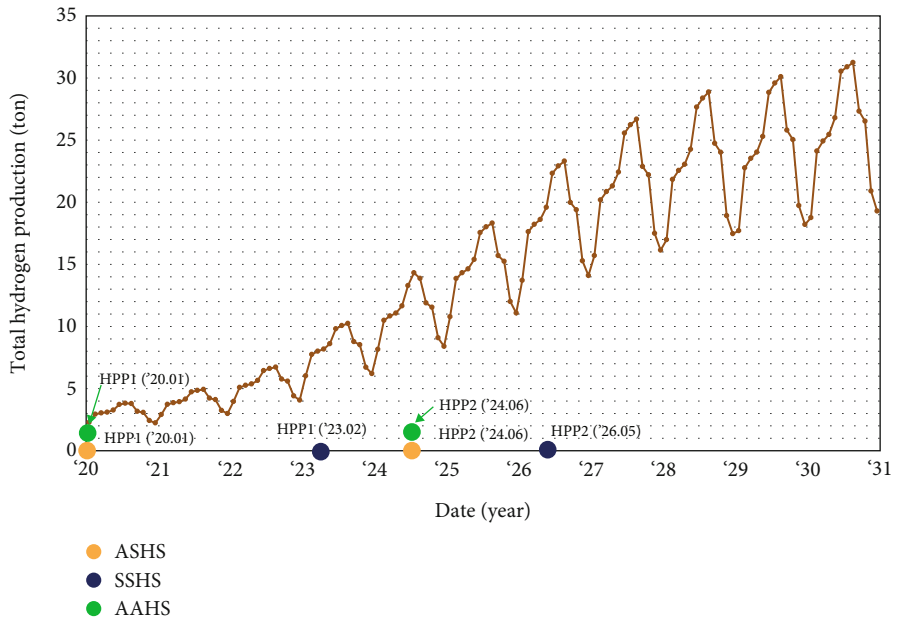

Figure 5: The investment point of the three proposed HPPs.

hydrogen demand has risen sharply over the years and inevitably requires an additional installation of an integrated hydrogen production system with HRS simultaneously. This could lead to a sudden increase in the investment cost for the hydrogen systems, where the optimal operation rate according to the number of integrated hydrogen production system with HRS should be determined to acquire economic benefit.

4.3. Optimal Operation Rate and Storage Tank Management. The investment timing to install HPP depends on the total hydrogen production through process operation rate based on the future hydrogen demand. Figure 5 shows the investment timing of each HPP for hydrogen production. ASHS and AAHS used HPP1 to produce hydrogen from the beginning and operated HPP2 in Jun. 2024 to meet future hydrogen demand. On the other hand, due to limited utilization rates, SSHS operated HPP1 for hydrogen production from Feb. 2023. The total hydrogen production was related to the operation rate and storage tank management for ASHS over the operating period of HPP.

In Figure S5 in SI, the ATR operation pattern shows a very similar tendency every year despite the increasing hydrogen demand. The level fluctuation in hydrogen storage tanks generally increases with an increase in the variability of the hydrogen demand. Hydrogen storage tanks are used to compensate for insufficient hydrogen production owing to hydrogen demand. Hence, even if the on-site hydrogen production system with HRS is composed, it is necessary to supplement the hydrogen supply by storing sufficient hydrogen for a long time considering hydrogen demand. In Figure S5 (a), hydrogen is first produced by ATR before it is produced by SMR, owing to lower hydrogen demand. SMR will be operated in

June 2024, when hydrogen production by ATR cannot satisfy hydrogen demand. The operation rate of SMR is maintained as much as possible considering the amount of hydrogen demand, and as hydrogen demand increases, the operating rate approaches 100%, and ATR is responsible for the insufficient hydrogen production quantities. The initial storage tank level is always maintained at maximum to cope with the volatility of hydrogen demand. In particular, the storage tank level depends on the hydrogen demand and the operating characteristics of the SMR. In addition, it has a significant fluctuation as the HPP begins to operate in dual-modal mode. In Figure S5 (b), SSHS is a system that purchases hydrogen and charges hydrogen vehicles from a hydrogen production system because it is difficult to operate in the early stages of hydrogen production owing to the operating condition constraints of SMR. The first SMR was operated to satisfy operating conditions in February 2023, and the second SMR was operated in June 2026. The SSHS also maintains a similar operation rate to the maximum possible extent, and the operation rate is changed by considering the operating conditions of each other. Rapid fluctuations in hydrogen demand simultaneously change the operating rates of the two SMRs and minimize the difference in their operating rates. The storage tank level of the SSHS generates fluctuation from a single operation mode due to the operation characteristics of the SMR. In Figure S5 (c), the operation rate and storage tank level of initial AAHS show a similar trend to ASHS by hydrogen production using ATR. The storage tank management of AAHS is maintained as the most stable owing to ATR's dual hydrogen production.

4.4. Economic Analysis Results. In general, total CAPEX and OPEX can depend significantly on the size of the production plant. The hydrogen production cost generally considers the initial investment, including equipment purchase and installation, to the operational costs during the overall lifetime. This study analyzed the economic feasibility of on-site HRS while satisfying the future hydrogen demand. The overall economic performance of each system was evaluated through cash flow, and the best systems with the lowest hydrogen production costs were identified. Hence, this study analyzes cash flow to determine the representative economic performance for operating the on-site hydrogen production system. The initial cash flow has a considerably high negative value owing to the low operation rate of the hydrogen production systems. However, by 2030, the operation rate of ASHS and AAHS will increase compared to 2020, and cash flows will reach a break-even point (BEP). In addition, the cash flow of the ASHS is lower than that of the other processes through the optimal production of hybrid ATR and SMR, considering hydrogen demand. The cash flow for the three proposed HPPs during the operation period is shown in Figure S6 in SI.

The total CAPEX consists of HPP, HRS, and CCS based on direct and indirect costs. CAPEX of HPP accounts for 43-45% of the total CAPEX. CAPEX of ASHS is similar to SSHS and is approximately 4% more expensive due to increased

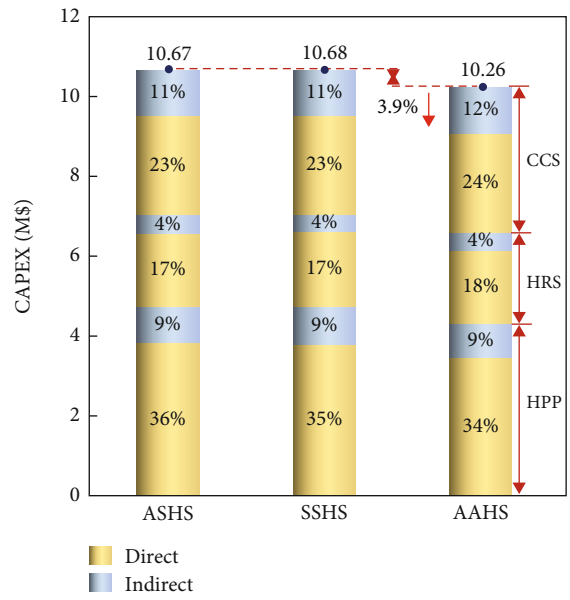

Figure 6: Comparison of CAPEX for three proposed HPPs.

equipment purchase costs than AAHS. Figure 6 presents the ratios of CAPEX for hydrogen production.

Figure 7 presents the cost contributions of the equipment for HPP and HRS in the three proposed HPPs. The CAPEX of the three proposed HPPs were almost identical. However, there is a difference in equipment depending on the operation mode. The reactor, PSA, and compressor in the three proposed HPPs account for approximately 40 −48% of the total CAPEX, and they are important equipment that determines investment costs. In particular, the operation modes with ATR also have ASU costs to supply high-purity oxygen.

Figure 8 presents the cost contributions of OPEX for three proposed HPPs. OPEX of three proposed HPPs depend on the purchase cost of raw materials. In particular, the costs of raw materials and labor account for an absolute percentage of approximately 66% of the total OPEX for three proposed HPPs. The OPEX of ASHS was lowest compared to SSHS and AAHS due to saving raw material purchase costs through optimal operational strategy. The raw materials cost of ASHS is lower by 8.0% and 15.4% compared to SSHS and AAHS, respectively. However, the operation mode with ATR requires more raw material than SMR because of the lower process efficiency. On the other hand, the HRS equipped with SSHS is not initially operated when the hydrogen production is less than the minimum operating rate and is operated by a system that purchases and charges hydrogen from outside. Hence, the OPEX of SSHS also includes GH_2 purchase cost. ASHS has the best economic feasibility from the perspective of process operation in on-site hydrogen production systems. Total OPEX of ASHS was lower by 4.4% and 10.3% compared to SSHS and AAHS.

Figure 9 presents a comparison of the LCOH for the three proposed HPPs over the total operation period. In general, the LCOH depends mainly on CAPEX, discount rate,

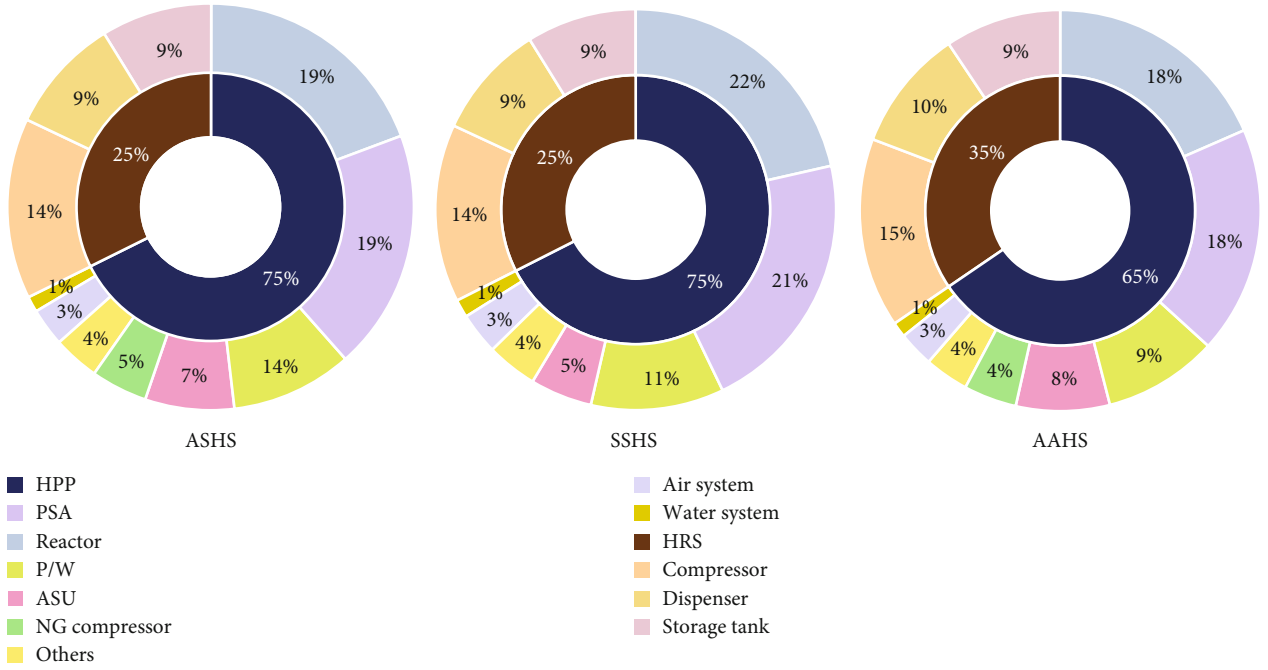

Figure 7: Investment and equipment cost distribution for three proposed HPPs.

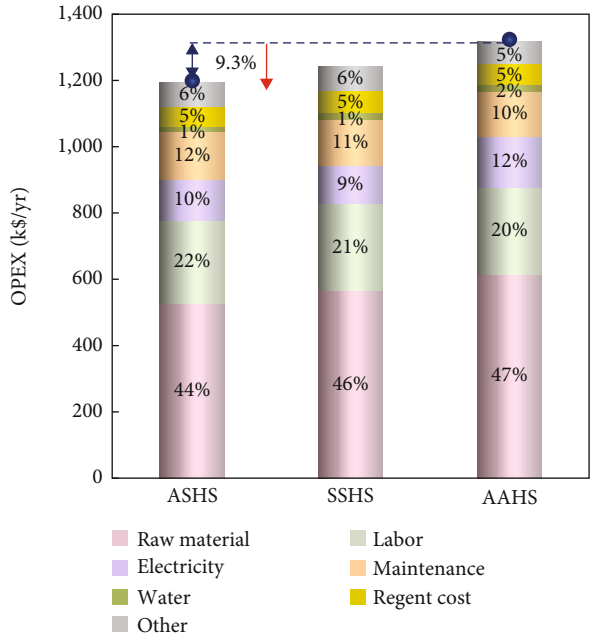

Figure 8: Cost distributions of OPEX for three proposed HPPs.

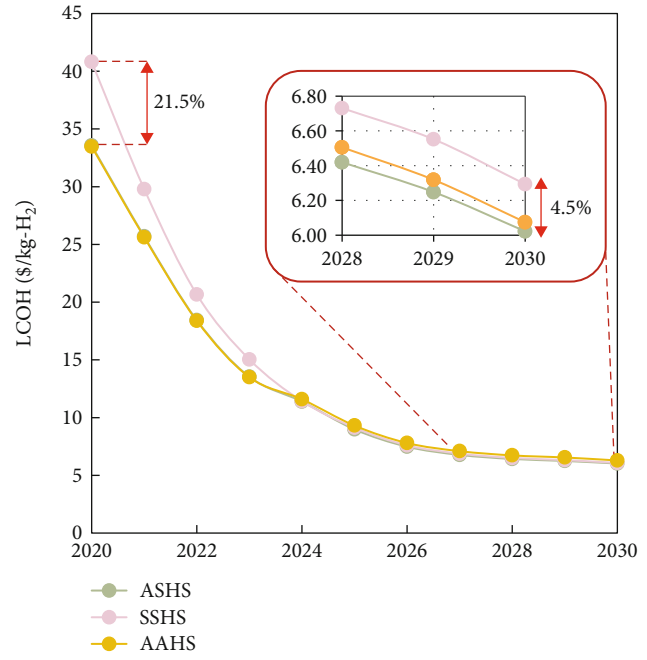

Figure 9: Comparison of LCOH for three proposed HPPs over the operation period.

and OPEX. All production processes in the early stages of hydrogen production have very high LCOH owing to the low hydrogen demand and process operation rate. However, the LCOH sharply decreases, and the operation rate of the hydrogen production process recovers as the hydrogen demand increases. In the case of SSHS, the initial LCOH is approximately 22.5 and 21.9% higher than ASHS and AAHS by the strategy of purchasing hydrogen from outside and charging the vehicles due to the limitation of the operation rate of the hydrogen production process. However, the LCOH of the ASHS and SSHS converges to a similar value (approximately \$6.02/kg H_2) when the process operation rate reaches a maximum value during the operation period. In particular, the LCOH difference between AAHS and SSHS will decrease to 4.5% by 2030. Furthermore, the price competitiveness of the SSHS was improved by an increase in hydrogen demand. Therefore, the SSHS might also be selected as an on-site hydrogen production with HRS considering the stable operation of the process and low CO_2 emissions.

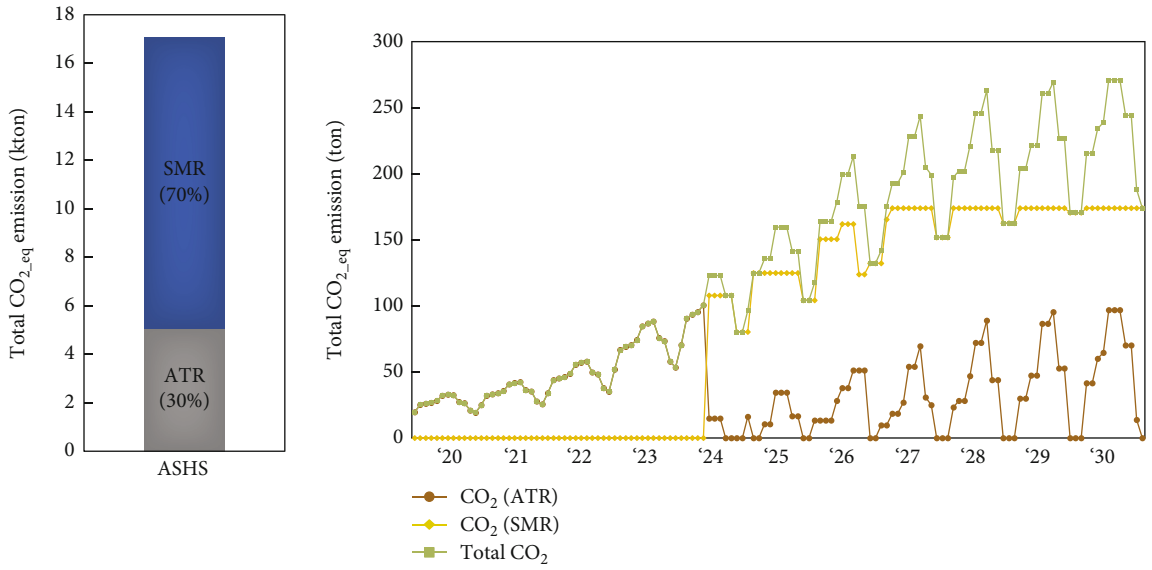

Figure 10: Comparison of CO_2 emissions for three proposed HPPs.

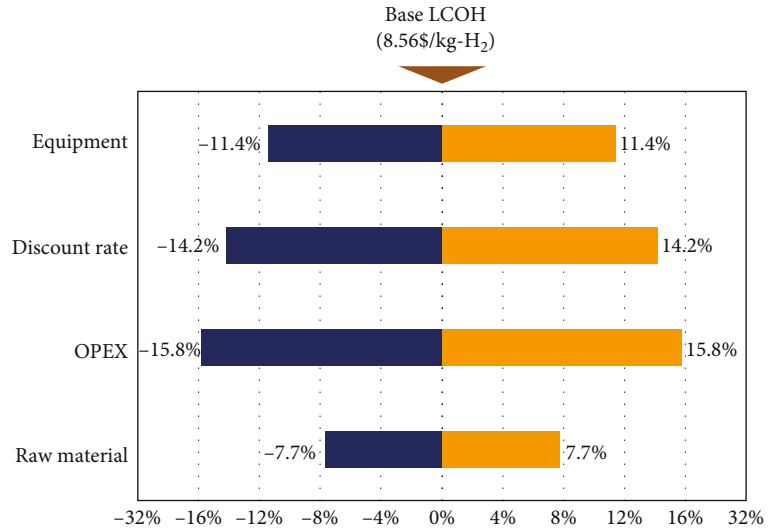

Figure 11: Sensitivity analysis for ASHS.

4.5. Environmental Analysis Results. CO_2 is significantly generated during the hydrogen production processes (most CO_2 emissions directly occur from SMR, ATR, and WGS processes) and NG combustion in the furnace. CO_2 generated from HPP could be dramatically reduced by capturing the majority of CO_2 at the purge streams, including tail gas from the process and exhaust gas from the furnace. Through this process, gray hydrogen could be converted to blue hydrogen. Figure 10 shows the amount of CO_2 emissions generated to produce GH_2. The amount of CO_2 emissions for three proposed HPPs (a, b, and c) are 8.9, 8.8, and 9.1 kg CO_2/kg H_2, respectively. Here, the SSHS has the lowest CO_2 emissions among the three proposed HPPs. This indicates that the initial CO_2 emissions of the SSHS are zero because hydrogen is not produced in the on-site hydrogen production system owing to the operation rate limitation. In addition, the CO_2 emissions of ASHS were lower by approximately 1.9% compared to AAHS. In general, although ATR has a lower process efficiency than SMR, it can reduce the amount of fuel required to maintain the reaction temperature through autothermal reactions, resulting in lower CO_2 emissions. However, ATR consumes more raw materials to produce the same amount of hydrogen because of its low process efficiency.

5. Sensitivity and Scenario Analysis

5.1. Sensitivity Analysis for Major Parameters. To analyze the key parameters affecting the LCOH, a sensitivity analysis was performed for the cost drivers, including equipment cost, discount rate, raw material purchase cost, and OPEX. The sensitivity analysis assumes a change of ±30% compared to the original parameters. Figure 11 shows the results of the

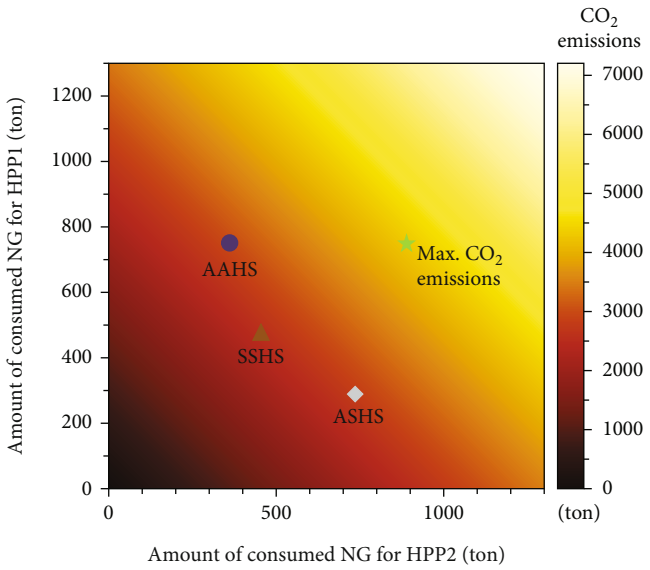

Figure 12: Comparison of CO_2 emissions for three proposed HPPs (2030) and the maximum case of hydrogen production (ASHS: HPP1-ATR and HPP2-SMR; SSHS: HPP1-SMR and HPP2-SMR; AAHS: HPP1-ATR and HPP2-ATR).

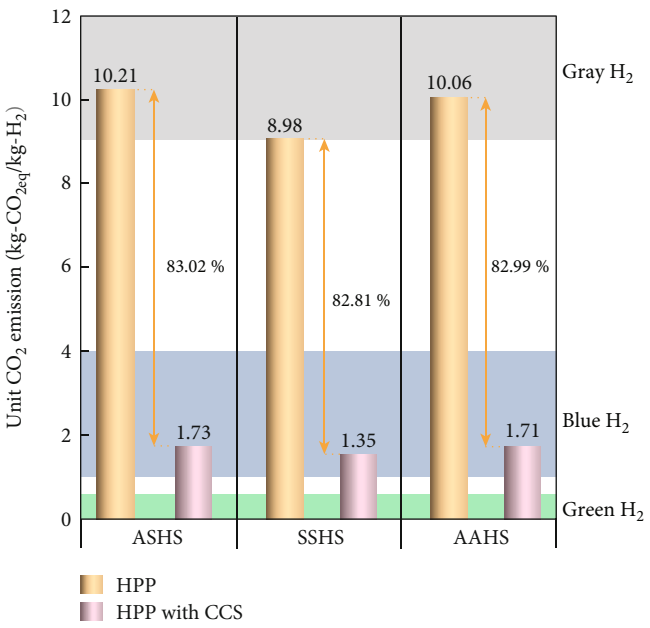

Figure 13: Comparison of unit CO_2 emissions between three proposed HPPs and the process with CCS.

sensitivity analysis of ASHS. OPEX is a more sensitive parameter than the other parameters because it is the dominant cost driver. Evidently, new technical improvements to lower operation costs using an optimal operation strategy can enhance the economic feasibility from GH_2 production to hydrogen charging based on the integrated on-site hydrogen production with HRS. In addition, the SSHS and AAHS show similar trends to ASHS in the sensitivity analysis for all the considered parameters.

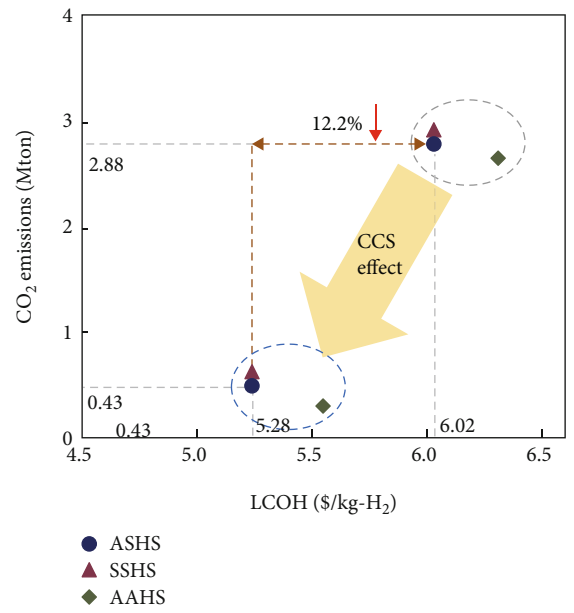

Figure 14: Comparison of the economic effects of three proposed HPPs through CCS (2030).

5.2. Comparison for CO_2 Emissions of Three Proposed HPPs. The amount of NG consumed by each HPP depends on the operation characteristics of SMR and ATR. Figure 12 shows the CO_2 emissions according to the maximum operation rate of HPPs and each proposed HPP as of 2030. In particular, the amount of NG consumed in the SMR of ASHS accounts for 72.7% of total consumption. If the amount of hydrogen production increases, ASHS requires maintaining the operation rate of hydrogen production due to the characteristics of SMR. The amount of NG consumed by each HPP in SSHS is similar because of dual operated by two SMRs. In AAHS, HPP1 consistently maintains the operation rate for hydrogen production, and HPP2 meets the hydrogen demand through variable operation.

5.3. Economic and Environmental Effect of Three Proposed HPPs with CCS. Currently, most countries are continuously making efforts to reduce CO_2 emissions. In this study, CCS was considered to reduce CO_2 emissions from hydrogen production facilities. Unit CO_2 emissions and LCOH of HPPs with CCS were compared with conventional HPPs. Figure 13 presents the comparison of unit CO_2 emissions, including generated CO_2 with CCS for the proposed HPPs. The CO_2 emissions were considerably reduced by CCS. The unit CO_2 emissions of three HPPs with CCS were decreased by approximately 83% compared to the proposed HPPs, at the values of 1.73, 1.35, and 1.71 kg CO_{2eq}/kg produced hydrogen, respectively. Hence, according to the reference, these values are included in the range of blue hydrogen [49].

Figure 14 shows the correlation between LCOH and CO_2 emissions from CCS capture and sales. In the case of ASHS, LCOH and CO_2 emissions as of 2030 are \$6.02/kg H_2 and 2.88 Mton, respectively. The LCOH of ASHS was increased due to equipment purchase and installation costs of CCS.

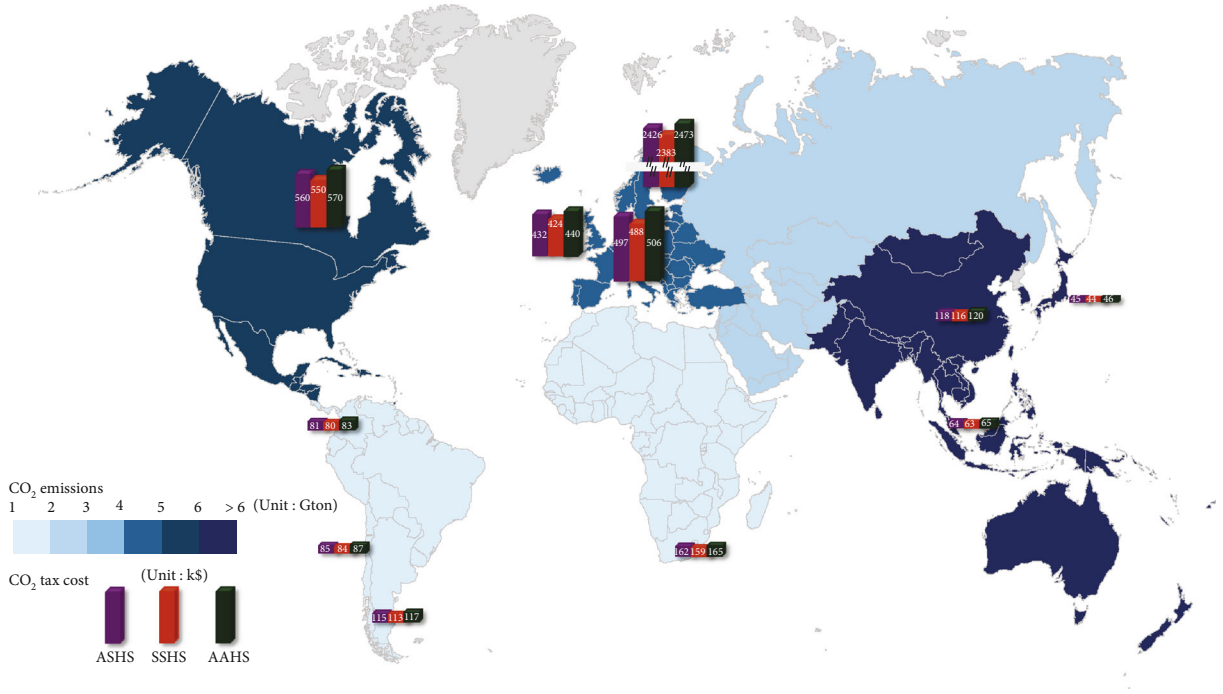

Figure 15: Comparison of carbon taxes by country for three proposed HPPs.

However, the final LCOH could be reduced by 12.2% through the sale of captured CO_2, and CO_2 emissions could also decrease by 2.45 Mton compared with ASHS without CCS.

5.4. Cost Analysis for Carbon Tax by Country. Carbon taxes around the world are implemented to compensate for the amount of GHGs released from industries into the Earth's atmosphere. To decelerate global warming, many developed and developing countries are planning to reach net zero emissions by 2050. Figure 15 shows the carbon tax based on the three HPPs when the carbon tax for each country is applied. In particular, the rates of carbon taxes vary significantly around the world. As shown in Figure 15, developed countries are more expensive than developing countries. In addition, Sweden has the highest carbon tax worldwide at approximately USD 2.38-2.47 million, while Japan has a carbon tax of less than USD 46 thousand. Carbon tax provides economic motivation for polluters to reduce GHGs or switch to more efficient processes and clean fuels.

6. Conclusion

This study proposed optimal investment strategies for three on-site hydrogen production with dual-modal modes based on hydrogen demand using a ML technique. The three HPPs consist of a combination of ATR-SMR, SMR-SMR, and ATR-ATR. This was done to determine the investment timing based on the optimal operation rate and storage tank management for the proposed HPPs. In addition, the three on-site HPPs were analyzed in terms of process, economic, and environmental impacts. In particular, the optimal operation rate and storage tank management were determined by satisfying hydrogen demand and various constraints. The R^2 and MSE values were obtained at 0.9936 and 6.88×10^{-5}, respectively. The CAPEX of ASHS is similar to SSHS and is approximately 4.0% higher than AAHS due to increased equipment purchase costs. However, the OPEX of ASHS could be reduced by 9.3% compared to AAHS through the optimal operation of HPPs. The profitability of the ASHS and SSHS was economically high in terms of long-term operation. However, the initial profitability and environmental impacts of SSHS were relatively low because of the operating rate limitations of hydrogen production systems. In addition, the CO_2 emissions of the ASHS were lower by 1.9% compared to AAHS. CO_2 generated from HPPs was decreased by approximately 83% using CCS, while LCOH was reduced by 12.2% through CO_2 sales. Furthermore, we investigated the economic and environmental effects of the three proposed HPPs with CCS. Moreover, the amount of NG consumed and CO_2 emissions generated in each HPP are analyzed using the 2030 operation rate relative to the maximum operation rate. These results contribute to establishing an optimal production strategy for maximizing the economic feasibility of hydrogen production systems.

Abbreviations

AAHS: Hydrogen production strategy of ATR-ATR dual modal mode process
ASHS: Hydrogen production strategy of ATR-SMR dual modal mode process
ANN: Artificial neural network
ASU: Air separation unit
ATR: Autothermal reforming
CAPEX: Capital expenditure
CEPCI: Chemical engineering plant cost index
CRF: Capital recovery factor

GHG: Greenhouse gas
GH_2: Gas hydrogen
HPP: Hydrogen production process
HRS: Hydrogen refueling station
HTS: High-temperature shift
LCA: Life cycle assessment
LCOH: Levelized cost of hydrogen
LNG: Liquefied natural gas
LTS: Low-temperature shift
NG: Natural gas
OPEX: Operating expenditure
PEMFC: Proton exchange membrane fuel cell
POX: Partial oxidation
PL: Plant life
PR: Prereformer
PSA: Pressure swing adsorption
SSHS: Hydrogen production strategy of SMR-SMR dual modal mode process
SMR: Steam methane reforming
TPD: Ton per day
WGS: Water gas shift.

Nomenclatures

Indice

j: Hydrogen production type.

Variables and parameters

AH_t: Amount of hydrogen sales during time period t
AR_t: Total amount of used raw material during time period t
$AF_{j,t}$: Amount of used NG to maintain reaction temperature of reactors by hydrogen production types j during time period t
APH_t: Amount of hydrogen production during time period t
$AP_{j,t}$: Amounts of produced hydrogen by hydrogen production types j during time period t
$AN_{j,t}$: Amounts of NG inputs by hydrogen production types j during time period t
C_a and C_b: Approximate and reference costs of main equipment
CL_t and CM_t: Labor and maintenance costs of hydrogen production systems and HRS during time period t
COT_t: The other costs during time period t
CR_t: The raw material price during time period t
$CR_{j,t}$: The conversion rates by hydrogen production types j during time period t
H_d: Predicted hydrogen demand
HS_t: The hydrogen selling price during time period t
HRS_{num}: The number of on-site hydrogen production with HRS
MP_t: Total profit during period t
n: The total number of considered data to learn ANN model
O_{hp}: Amount of one on-site hydrogen production
OC_t: Operating cost during time period t
$OR_{j,t}$: The operation rates by hydrogen production types j during time period t
$OR_t^{SMR,L}$ and $OR_t^{SMR,U}$: The lower and upper bounds of operation rate to SMR during time period t
$OR_t^{ATR,L}$ and $OR_t^{ATR,U}$: The lower and upper bounds of operation rate to ATR during time period t
P_{H_2}: Total amount of produced hydrogen during time period t
RM_t: The raw material cost during time period t
S: The standard deviation of the data
S_b and S_a: Target and reference sizes of main equipment
TI_t: The annualized total investment cost during time period t
TP_t: The total profit during time period t
RM_t: The raw material cost during time period t
TS_t: Amount of stored hydrogen in the storage tank during time period t
TS_{t-1}: Amount of stored hydrogen in the storage tank from the previous month during time period t
α: Scaling factor
i: Discount rate
x_i: The data points of the descriptor i
$\bar{x}$: The mean of the data
y_i and $\hat{y}_i$: The actual and predicted values of the ith data
$\bar{y}_i$: The average value of total data.

Data Availability

No data was used for the research described in the article.

Conflicts of Interest

The authors declare that they have no known competing financial interests or personal relationships that could have influenced the work reported in this study.

Authors' Contributions

Hweeung Kwon was responsible for the conceptualization, methodology, formal analysis, and writing. Jinwoo Park was responsible for the investigation, visualization, formal analysis, and software. Jae Eun Shin was responsible for the formal analysis, writing, and editing. Bonchan Koo was responsible for the supervision, conceptualization, visualization, review, and editing. Jinwoo Park, Jae Eun Shin, and Bonchan Koo have the same contribution to this study.

Acknowledgments

This work was supported by the Soonchunhyang University Research Fund (20231284). This research was supported by the Basic Research Project (Development of Carbon Reduced Reservoir Management Technologies for Blue Hydrogen Production, 24-3314) of the Korea Institute of Geoscience and Mineral Resources (KIGAM) funded by the Ministry of Science and ICT. Furthermore, this work was supported by the Industrial Technology Innovation Program (RS-2022-00143883, "Carbon Reduction Process Design Model Development") funded by the Ministry of Trade, Industry & Energy (MOTIE, Korea).

Supplementary Materials

Figure S1: schematic block diagram of a proposed representative system for hydrogen production. Figure S2: process flow diagram of SSHS process. Figure S3: process flow diagram of AAHS process. Figure S4: number of hydrogen production system with HRS based on the predicted hydrogen demand. Figure S5: optimal operation rate and storage tank management of three proposed HPPs for hydrogen production ((a) ASHS, (b) SSHS, (c) AAHS). Figure S6: comparison of the cash flow for three proposed HPPs over the operation period. Figure S7: comparison of CO_2 emissions for SSHS and AAHS processes. Table S1: major descriptors to predict hydrogen demand. Table S2: stream information of ASHS process. Table S3: stream information of SSHS process. Table S4: stream information of AAHS process. Table S5: the lower and upper bound values of the storage tank and operation rates of SMR. (*Supplementary Materials*) *(Supplementary Materials)*

References

[1] M. Ball and M. Wietschel, "The future of hydrogen-opportunities and challenges," *International Journal of Hydrogen Energy*, vol. 34, no. 2, pp. 615–627, 2009.

[2] P. P. Edwards, V. L. Kuznetsov, W. I. F. David, and N. P. Brandon, "Hydrogen and fuel cells: towards a sustainable energy future," *Energy Policy*, vol. 36, no. 12, pp. 4356–4362, 2008.

[3] M. Ball and M. Weeda, "The hydrogen economy—vision or reality?," *Compendium of Hydrogen Energy*, vol. 4, pp. 237–266, 2016.

[4] M. V. Twigg, *Catalyst Handbook*, Wolfe Publishing Ltd, London, 2nd edition, 1989.

[5] M. Onozaki, K. Watanabe, T. Hashimoto, H. Saegusa, and Y. Katayama, "Hydrogen production by the partial oxidation and steam reforming of tar from hot coke oven gas," *Fuel*, vol. 85, no. 2, pp. 143–149, 2006.

[6] J. M. Ogden, M. M. Steinbugler, and T. G. Kreutz, "Comparison of hydrogen, methanol and gasoline as fuels for fuel cell vehicles: implications for vehicle design and infrastructure development," *Journal of Power Sources*, vol. 79, no. 2, pp. 143–168, 1999.

[7] R. Farrauto, S. Hwang, L. Shore et al., "New material needs for hydrocarbon fuel processing: generating hydrogen for the PEM fuel cell," *Annual Review of Materials Research*, vol. 33, no. 1, pp. 1–27, 2003.

[8] C. Song, "Fuel processing for low-temperature and high-temperature fuel cells challenges, and opportunities for sustainable development in the 21st century," *Catalysis Today*, vol. 77, no. 1-2, pp. 17–49, 2002.

[9] B. Sorensen, "Vision hydrogen fuel cell truck for TTSI, 100 on order," *Fuel Cells Bulletin*, vol. 2011, no. 8, p. 2, 2011.

[10] D.-H. Kim, S.-H. Kim, I.-B. Ko, C.-Y. Lee, and H.-S. Shin, "Start-up strategy for continuous fermentative hydrogen production: early switchover from batch to continuous operation," *International Journal of Hydrogen Energy*, vol. 33, no. 5, pp. 1532–1541, 2008.

[11] M. Kiaee, A. Cruden, P. Chadek, and D. Infield, "Demonstration of the operation and performance of a pressurised alkaline electrolyser operating in the hydrogen fuelling station in Porsgrunn, Norway," *Energy Conversion and Management*, vol. 94, pp. 40–50, 2015.

[12] M. Genovese, D. Blekhman, M. Dray, and P. Fragiacomo, "Hydrogen losses in fueling station operation," *Journal of Cleaner Prodroduction*, vol. 248, article 119266, 2020.

[13] D. Xu, Z.-H. Yuan, Z. Bai, Z. Wu, S. Chen, and M. Zhou, "Optimal operation of geothermal-solar-wind renewables for community multi-energy supplies," *Energy*, vol. 249, article 123672, 2022.

[14] S. Samsatli, I. Staffell, and N. J. Samsatli, "Optimal design and operation of integrated wind-hydrogen-electricity networks for decarbonising the domestic transport sector in Great Britain," *International Journal of Hydrogen Energy*, vol. 41, no. 1, pp. 447–475, 2016.

[15] M. Kim and J. Kim, "An integrated decision support model for design and operation of a wind-based hydrogen supply system," *International Journal of Hydrogen Energy*, vol. 42, no. 7, pp. 3899–3915, 2017.

[16] J. Liu, Z. Xu, J. Wu, K. Liu, and X. Guan, "Optimal planning of distributed hydrogen-based multi-energy systems," *Applied Energy*, vol. 281, article 116107, 2021.

[17] X. Wu, S. Qi, Z. Wang, C. Duan, X. Wang, and F. Li, "Optimal scheduling for microgrids with hydrogen fueling stations considering uncertainty using data-driven approach," *Applied Energy*, vol. 253, article 113568, 2019.

[18] D. Jang, J. Kim, D. Kim, W. Han, and S. Kang, "Techno-economic analysis and Monte Carlo simulation of green hydrogen production technology through various water electrolysis technologies," *Energy Conversion and Management*, vol. 258, article 115499, 2022.

[19] J. C. Restrepo, D. L. Lzidoro, A. M. L. Nasner, O. J. Venturini, and E. E. S. Lora, "Techno-economical evaluation of renewable hydrogen production through concentrated solar energy," *Energy Conversion and Management*, vol. 258, article 115372, 2022.

[20] R. Soltani, M. A. Rosen, and I. Dincer, "Assessment of CO_2 capture options from various points in steam methane reforming for hydrogen production," *International Journal of Hydrogen Energy*, vol. 39, no. 35, pp. 20266–20275, 2014.

[21] G. Power, A. Busse, and J. MacMurray, "Demonstration of carbon capture and sequestration of steam methane reforming process gas used for large-scale hydrogen production," in *Final report*, Air Products and Chemicals, Inc., 2018, DE-FE002381.

[22] P. L. Spath and M. K. Mann, *Life cycle assessment of hydrogen production via natural gas steam reforming*, National Renewable Energy Laboratory, 2000, TP 570-27637.

[23] A. Elgowainy, J. Han, and H. Zhu, *Updates to parameters of hydrogen production pathways in GREET™*, Argonne National Laboratory, 2013.

[24] A. O. Oni, K. Giwa, G. D. Lullo, and A. Kumar, "Comparative assessment of blue hydrogen from steam methane reforming, autothermal reforming, and natural gas decomposition technologies for natural gas-producing regions," *Energy Conversion and Management*, vol. 254, article 115245, 2022.

[25] M. Granovskii, I. Dincer, and M. A. Rosen, "Greenhouse gas emissions reduction by use of wind and solar energies for hydrogen and electricity production: economic factors," *International Journal of Hydrogen Energy*, vol. 32, no. 8, pp. 927–931, 2007.

[26] C. Acar and I. Dincer, "Comparative assessment of hydrogen production methods from renewable and non-renewable sources," *International Journal of Hydrogen Energy*, vol. 39, no. 1, pp. 1–12, 2014.

[27] C. Acar and I. Dincer, "Review and evaluation of hydrogen production options for better environment," *Journal of Cleaner Production*, vol. 218, pp. 835–849, 2019.

[28] S. Hong, J. Lee, H. Cho, M. Kim, I. Moon, and J. Kim, "Multi-objective optimization of CO_2 emission and thermal efficiency for on-site steam methane reforming hydrogen production process using machine learning," *Journal of Cleaner Production*, vol. 359, article 132133, 2022.

[29] J. Lee, S. Hong, H. Cho et al., "Machine learning-based energy optimization for on-site SMR hydrogen production," *Energy Conversion and Management*, vol. 244, article 114438, 2021.

[30] D. Strusnic and J. Avsec, "Exergoeconomic machine-learning method of integrating a thermochemical cu-cl cycle in a multi-generation combined cycle gas turbine for hydrogen production," *International Journal of Hydrogen Energy*, vol. 47, no. 39, pp. 17121–17149, 2022.

[31] Z. Haq, H. Ullah, M. N. A. Khan, S. R. Naqvi, and M. Ahsan, "Hydrogen production optimization from sewage sludge supercritical gasification process using machine learning methods integrated with genetic algorithm," *Chemical Engineering Research and Design*, vol. 184, pp. 614–626, 2022.

[32] M. Pourali and J. A. Esfahani, "Performance analysis of a micro-scale integrated hydrogen production system by analytical approach, machine learning, and response surface methodology," *Energy*, vol. 255, article 124553, 2022.

[33] E. E. Ozbas, D. Aksu, A. Ongen, M. A. Aydin, and H. K. Ozcan, "Hydrogen production via biomass gasification, and modeling by supervised machine learning algorithms," *International Journal of Hydrogen Energy*, vol. 44, no. 32, pp. 17260–17268, 2019.

[34] N. D. Vo, D. H. Oh, S. H. Hong, M. Oh, and C. H. Lee, "Combined approach using mathematical modelling and artificial neural network for chemical industries: steam methane reformer," *Applied Energy*, vol. 255, article 113809, 2019.

[35] B. Koo, T. Jo, and D. Lee, "Modified inferential POD/ML for data-driven inverse procedure of steam reformer for 5-kW HT-PEMFC," *Compututers & Chemical Engineering*, vol. 121, pp. 375–387, 2019.

[36] E. S. Hecht and J. Pratt, *Comparison of conventional vs. modular hydrogen refueling stations, and on-site production vs. delivery*, NREL, 2017, DE-AC36-08GO28308.

[37] H.-M. Wang, K.-S. Choi, I.-H. Kang, H.-M. Kim, and P. A. Erickson, "Theoretical analyses of autothermal reforming methanol for use in fuel cell," *Journal of Mechanical Science and Technology*, vol. 20, no. 6, pp. 864–873, 2006.

[38] M. E. E. Abashar, K. I. Alhumaizi, and A. M. Adris, "Investigation of methane-steam reforming in fluidized bed membrane reactors," *Chemical Engineering Research and Design*, vol. 81, no. 2, pp. 251–258, 2003.

[39] H. H. Faheem, H. U. Tanveer, S. Z. Abbas, and F. Maqbool, "Comparative study of conventional steam-methane-reforming (SMR) and auto-thermal-reforming (ATR) with their hybrid sorption enhanced (SE-SMR & SE-ATR) and environmentally benign process models for the hydrogen production," *Fuel*, vol. 297, article 120769, 2021.

[40] Y. Choi and H. G. Stenger, "Water gas shift reaction kinetics and reactor modeling for fuel cell grade hydrogen," *Journal of Power Sources*, vol. 124, no. 2, pp. 432–439, 2003.

[41] M. J. Azarhoosh, H. A. Ebrahim, and S. H. Pourtarah, "Simulating and optimizing hydrogen production by low-pressure autothermal reforming of natural gas using non-dominated sorting genetic algorithm-II," *Chemical and Biochemical Engineering Quarterly*, vol. 29, no. 4, pp. 519–531, 2016.

[42] F. Khademi, M. Akbari, S. M. Jamal, and M. Nikoo, "Multiple linear regression, artificial neural network, and fuzzy logic prediction of 28 days compressive strength of concrete," *Frontiers of Structural and Civil Engineering*, vol. 11, no. 1, pp. 90–99, 2017.

[43] H. Tabari, A.-A. Sabziparvar, and M. Ahmadi, "Comparison of artificial neural network and multivariate linear regression methods for estimation of daily soil temperature in an arid region," *Meteorollgy and Atmospheric Physics*, vol. 110, no. 3-4, pp. 135–142, 2011.

[44] S. Sharma and A. Athaiya, "Activation functions in neural networks," *International Journal of Applied Science and Technology*, vol. 4, no. 12, pp. 310–316, 2020.

[45] S. C. Kim, S. H. Lee, and K. B. Yoon, "Thermal characteristics during hydrogen fueling process of type IV cylinder," *International Journal of Hydrogen Energy*, vol. 35, no. 13, pp. 6830–6835, 2010.

[46] J.-H. Yang, Y. Yoon, M. Ryu, S.-K. An, J. Shin, and C.-J. Lee, "Integrated hydrogen liquefaction process with steam methane reforming by using liquefied natural gas cooling system," *Applied Energy*, vol. 255, article 113840, 2019.

[47] B. J. Kim, W. L. Yoon, and D. J. Seo, "Analysis of the economy of scale for domestic steam methane reforming hydrogen refueling stations utilizing the scale factor," *Transactions of Korean Hydrogen and New Energy Society*, vol. 30, no. 3, pp. 251–259, 2019.

[48] T. N. Do and J. Kim, "Green C_2-C_4 hydrocarbon production through direct CO_2 hydrogenation with renewable hydrogen: process development and techno-economic analysis," *Energy Conversion and Management*, vol. 214, article 112866, 2020.

[49] A. Ajanovic, M. Sayer, and R. Haas, "The economics and the environmental benignity of different colors of hydrogen," *International Journal of Hydrogen Energy*, vol. 47, no. 57, pp. 24136–24154, 2022.